The Plant Cell, Vol. 18, 2194–2206, September 2006, www.plantcell.org © 2006 American Society of Plant Biologists

Tobacco WLIM1 Is a Novel F-Actin Binding Protein Involved in Actin Cytoskeleton Remodeling[W]

Clément Thomas,[a,1,2] Céline Hoffmann,[a,1] Monika Dieterle,[a] Marleen Van Troys,[b] Christophe Ampe,[b] and André Steinmetz[a,c]

[a] Centre de Recherche Public-Santé, L-1526 Luxembourg
[b] Department of Biochemistry, Faculty of Medicine and Health Sciences, Ghent University and Medical Protein Research, Flanders Interuniversity Institute for Biotechnology, B-9052 Gent, Belgium
[c] Institut de Biologie Moléculaire des Plantes, Centre National de la Recherche Scientifique, F-67084 Strasbourg, France

We used confocal microscopy and in vitro analyses to show that *Nicotiana tabacum* WLIM1, a LIM domain protein related to animal Cys-rich proteins, is a novel actin binding protein in plants. Green fluorescent protein (GFP)–tagged WLIM1 protein accumulated in the nucleus and cytoplasm of tobacco BY2 cells. It associated predominantly with actin cytoskeleton, as demonstrated by colabeling and treatment with actin-depolymerizing latrunculin B. High-speed cosedimentation assays revealed the ability of WLIM1 to bind directly to actin filaments with high affinity. Fluorescence recovery after photobleaching and fluorescence loss in photobleaching showed a highly dynamic in vivo interaction of WLIM1-GFP with actin filaments. Expression of WLIM1-GFP in BY2 cells significantly delayed depolymerization of the actin cytoskeleton induced by latrunculin B treatment. WLIM1 also stabilized actin filaments in vitro. Importantly, expression of WLIM1-GFP in *Nicotiana benthamiana* leaves induces significant changes in actin cytoskeleton organization, specifically, fewer and thicker actin bundles than in control cells, suggesting that WLIM1 functions as an actin bundling protein. This hypothesis was confirmed by low-speed cosedimentation assays and direct observation of F-actin bundles that formed in vitro in the presence of WLIM1. Taken together, these data identify WLIM1 as a novel actin binding protein that increases actin cytoskeleton stability by promoting bundling of actin filaments.

INTRODUCTION

The actin cytoskeleton is a highly organized and dynamic structure present in all eukaryotic cells where it plays a central role in many processes, including intracellular transport, cell growth, signaling, and division. Its assembly from monomeric subunits (G-actin) requires energy, and the resulting filamentous structure is stabilized by a subset of actin binding proteins (ABPs) that bind along the side of the filament. The presence of these proteins also affects the cytoskeletal structure and architecture by mediating the association of actin filaments into cables and bundles and cross-linking these structures into complex networks. ABPs not only regulate the supramolecular organization and function of the actin cytoskeleton but they also control its dynamics via polymerization/depolymerization and severing (McCurdy et al., 2001). In plants, several ABPs have been described, including monomer binding proteins (e.g., profilins; Staiger et al., 1993), severing and dynamizing proteins (e.g., ADF/cofilins; Dong et al., 2001; Chen et al., 2002), and side binding proteins (e.g., fimbrin [Kovar et al., 2000], 135-ABP/villin [Vidali et al., 1999], and 115-ABP/villin [Yokota et al., 2003]). The data presented here demonstrate that the tobacco (*Nicotiana tabacum*) LIM domain–containing protein WLIM1 is an ABP that participates in actin cytoskeleton remodeling possibly by promoting actin bundling.

The LIM domain, basically consisting of two zinc fingers linked together by a short two–amino acid spacer, is found in a wide variety of eukaryotic proteins and functions as a protein–protein interaction module (Schmeichel and Beckerle, 1997). Whereas animal genomes encode numerous LIM domain–containing proteins (LIMs) of diverse structures and functions (Kadrmas and Beckerle, 2004), plants only contain a limited number of LIMs, a majority of which, including tobacco WLIM1, belongs to the Cys-rich protein (CRP) LIM subfamily (Baltz et al., 1992; Eliasson et al., 2000). CRP-related proteins have also been identified in insects (Stronach et al., 1996) and protozoa (Khurana et al., 2002), indicating that these proteins participate in important evolutionarily conserved eukaryotic cellular mechanisms. Plant LIMs and vertebrate CRPs are small proteins of ~200 amino acids that display the same overall architecture, comprising two very similar LIM domains with >50% sequence identity, separated by a 40- to 50-residue-long spacer. Vertebrate CRPs have been found to accumulate in both the nucleus and the cytoplasm where they associate with the actin cytoskeleton (Arber and Caroni, 1996). Because of their ability to bind to zyxin (Sadler et al., 1992) and α-actinin (Pomiès et al., 1997), two actin cytoskeleton-associated proteins, and because of the absence of any known actin binding motif in their sequences, the

[1] These authors contributed equally to this work.
[2] To whom correspondence should be addressed. E-mail clement.thomas@crp-sante.lu; fax 352-26-970-390.
The author responsible for distribution of materials integral to the findings presented in this article in accordance with the policy described in the Instructions for Authors (www.plantcell.org) is: André Steinmetz (andre.steinmetz@crp-sante.lu).
[W] Online version contains Web-only data.
www.plantcell.org/cgi/doi/10.1105/tpc.106.040956

association of the CRPs with the actin cytoskeleton was believed to be indirect rather than direct. However, recently, CRP1 and CRP2 were shown to interact directly with F-actin (Grubinger and Gimona, 2004; Tran et al., 2005). In addition, in vitro data strongly suggest that CRP1 is an important cellular regulator of actin filament bundling (Tran et al., 2005).

Plant CRP-like LIMs have also been reported to display a dual nuclear-cytoplasmic distribution (Mundel et al., 2000), supporting the view that, like vertebrate CRPs, they participate in cytoplasmic and nuclear functions. In mature sunflower (*Helianthus annuus*) pollen grains, mRNAs encoding LIM proteins make up ~3% of the total mRNA population (Eliasson et al., 2000) and are therefore among the most abundant pollen transcripts. In other organs of the plant, LIM protein mRNAs are much less abundant (0.005 to 0.03% of the mRNAs). Immunocytological analyses have shown that sunflower PLIM1 concentrates in the germination cones of mature pollen grains, a region that also contains high amounts of F-actin (Baltz et al., 1999). Together, these observations suggest that some of the plant LIM proteins participate in pollen tube growth, a process that involves very active actin cytoskeleton remodeling and the formation and stabilization of long actin cables (Kost et al., 1998; Vidali et al., 2001; Chen et al., 2002). However, direct evidence for an interaction between plant LIMs and the actin cytoskeleton is still missing, and the functions of plant LIM proteins remain unclear. Moreover, the situation is rather confusing since an interaction between the sunflower LIM protein WLIM1 and microtubules in sunflower protoplasts has been suggested (Brière et al., 2003).

We describe here the subcellular localization in tobacco Bright Yellow 2 (BY2) cells of the tobacco protein WLIM1 fused to green fluorescent protein (WLIM1-GFP) as analyzed by laser scanning confocal microscopy. Like other CRP and CRP-related proteins, tobacco WLIM1 has a dual nuclear and cytoplasmic distribution. In the cytoplasm, WLIM1-GFP was found to associate with the actin cytoskeleton during both interphase and mitosis. In vitro experiments demonstrated the ability of WLIM1-GFP to bind directly to F-actin independently of any other intermediary protein and to stabilize actin filaments. Expression of WLIM1-GFP in *Nicotiana benthamiana* leaf cells modifies the normal actin cytoskeleton architecture by promoting the recruitment of actin filaments into thick actin bundles and cables. Similar structures can be induced in vitro by copolymerizing actin filaments with recombinant WLIM1. Possible biological roles for WLIM1 and plant LIMs are discussed.

RESULTS

WLIM1 Is Not Expressed in Tobacco BY2 Cells

Earlier studies had shown that the tobacco WLIM1 gene is expressed in various organs of the tobacco plant, including leaves, stems, and young and mature anthers, but not in pollen grains (Eliasson et al., 2000). Transcripts were also detected in pistils but in much lower amounts than in the other vegetative tissues, suggesting a differential expression of the gene in the various vegetative cell types. The use of tobacco BY2 cells as an expression system in this study therefore prompted us to verify whether these cells contain an endogenous WLIM1 protein or not, since an ectopic expression could potentially generate cells with a specific phenotypic marker, thus giving hints regarding the protein's function. RT-PCR amplification using a WLIM1-specific primer pair showed that the gene is not expressed in BY2 cells (see Supplemental Figure 1 online). Only transcripts encoding another tobacco LIM protein, WLIM2, whose coding sequence was originally isolated from a BY2 cDNA library (W.H. Shen and C. Gigot, unpublished data), were detected.

WLIM1 Colocalizes with the Actin Cytoskeleton

To study the subcellular localization of WLIM1, N- and C-terminal fusions with GFP were expressed under the control of the pUAS-Gal4 glucocorticoid-inducible promoter (Aoyama and Chua, 1997) in BY2 cells stably transformed using *Agrobacterium tumefaciens*–mediated transformation. The two types of fusions showed an identical distribution, indicating that the fused GFP does not interfere with the binding of the protein to its normal target. We present here the results for WLIM1 fused C-terminally to GFP. Figure 1A shows several cells of a stably transformed clone 24 h after induction. WLIM1-GFP was detected in the cytoplasm associated with a filamentous network and at low levels in the nucleus (Figure 1B). The filaments were frequently arrayed longitudinally along the elongation axis, but a cortical network at times transversally oriented could also be observed. Rhodamine-phalloidin labeling of the induced cells revealed that WLIM1 colocalizes with the actin cytoskeleton (Figures 2A to 2C). We noticed that Nonidet P-40, present in the rhodamine-phalloidin reaction buffer, induced artifacts in LIM localization

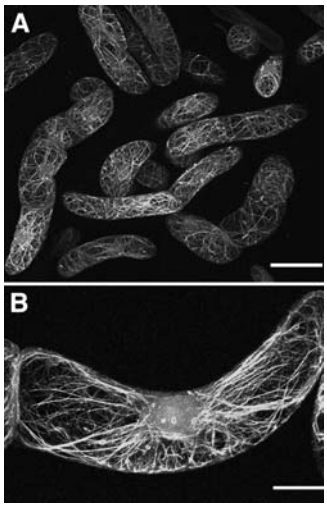

Figure 1. Induced Expression of the GFP-WLIM1 Fusion Protein in Tobacco BY2 Cells.

BY2 cells stably transformed with pTA7002-WLIM1-GFP were induced with dexamethasone and observed between microscope slides. **(A)** and **(B)** represent projections of x, y, and z optical 0.45-μm sections, respectively.

(A) Global view of the population of WLIM1-GFP–expressing cells. Bar = 50 μm.

(B) Enlarged view of a cell showing transcytoplasmic fluorescent filaments and a weak, diffuse nuclear fluorescence. Bar = 10 μm.

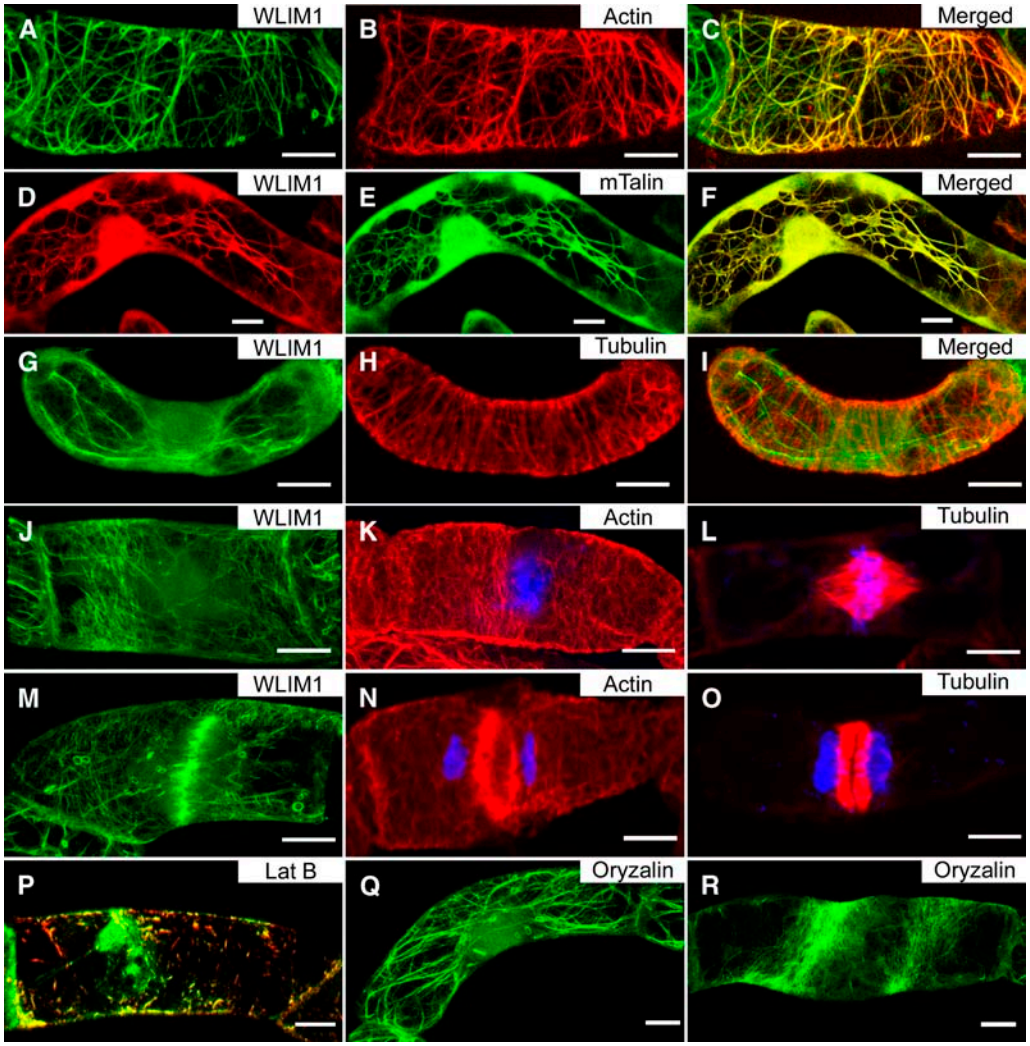

Figure 2. WLIM1 Binding to Actin Filaments.

Colabeling experiments of WLIM1-GFP, actin, and tubulin in BY2 cells. Images represent projections of x, y, and z optical 0.45-μm sections, respectively. Bars = 10 μm.

(A) to **(C)** Induced cells containing WLIM1 green fluorescent filaments **(A)** were labeled with rhodamine-phalloidin (red signal; **[B]**). WLIM1-GFP and actin filaments colocalize as judged by the presence of yellow filaments in the merged image **(C)**.

(D) to **(F)** Induced BY2 cells coexpressing mRFP-WLIM1 **(D)** and YFP-Talin **(E)**. Merged image is shown in **(F)**.

(G) to **(I)** Localization of WLIM1-GFP **(G)** after fixation and immunolabeling with an antitubulin antibody and a goat anti-mouse Alexa 568 secondary antibody **(H)**. Merged image is shown in **(I)**.

(J) to **(O)** Localization of WLIM1-GFP during the cell cycle. Metaphase cell (**[J]** to **[L]**): WLIM1-GFP **(J)**, actin (rhodamine-phalloidin; **[K]**), and tubulin (immunolabeling; **[L]**). Telophase cell (**[M]** to **[O]**): WLIM1-GFP **(M)**, actin **(N)**, and tubulin **(O)**. Chromosomes are stained with 4′,6-diamidino-2-phenylindole (DAPI) (in blue).

(P) to **(R)** Sensitivity of WLIM1 to cytoskeletal drugs.

(P) Effect of an 18-h treatment with LatB (200 nM): merged image of WLIM1-GFP cells stained with rhodamine-phalloidin.

(Q) and **(R)** Effect of an 18-h treatment with oryzalin (10 μM). Organization of WLIM1-GFP in 87% of the population **(Q)** and in 13% of the cells **(R)**. The latter cells are blocked in metaphase due to microtubule depolymerization.

after a few minutes of incubation, allowing only a narrow time window during which colocalization of the LIM protein and the actin network could be observed. Past this window WLIM1-GFP was released from the actin filaments and accumulated in the nucleus and in the mitotic microtubule spindle of dividing cells (data not shown). Triton was found to produce similar artifacts.

As an alternative, we also produced transgenic BY2 cell lines coexpressing the WLIM1 protein fused to the red fluorescent protein (mRFP-WLIM1) and the actin binding domain of the mouse talin fused to yellow fluorescent protein (YFP-mTalin), which is known to decorate the filamentous actin (Kost et al., 1998). The merge (Figure 2F) of the mRFP-WLIM1 (Figure 2D)

and YFP-mTalin (Figure 2E) signals confirms that WLIM1 localizes to the actin cytoskeleton.

To check for any possible interaction between WLIM1 and microtubules, transgenic WLIM1-GFP–expressing BY2 cells were fixed and subjected to microtubule immunolocalization using a detergent-free procedure. As shown in the merged image (Figure 2I), WLIM1 (Figure 2G) and microtubules (Figure 2H) do not colocalize.

A statistical analysis revealed that ~5% of the cells expressing the WLIM1-GFP fusion protein exhibited a different GFP pattern than the rest of the population (Figures 2J and 2M). Using differential interference contrast microscopy, these cells were found to present a nuclear structure typical of a mitotic nucleus (data not shown). This 5% ratio of dividing cells is in agreement with the one previously reported by Nagata et al. (1992) for a nonsynchronized BY2 cell culture. During metaphase, WLIM1 is organized in a thin cortical network with a WLIM1-depleted zone around the nucleus (Figure 2J). This pattern is consistent with the metaphase actin cytoskeleton organization (Figure 2K), while at the same stage, microtubules concentrate in the mitotic spindle (Figure 2L). Figure 2M shows the typical WLIM1-GFP network observed during telophase. The high accumulation of WLIM1-GFP in a ring structure at the cell center is striking, as it resembles the phragmoplast, an actin-rich structure of dividing cells (Figure 2N). By contrast, microtubules form a typical barrel structure between the two nuclei (Figure 2O). The unmarked thin band corresponds to the plate position at which periphery WLIM1-GFP and F-actin accumulate (Figures 2M and 2N). Together, these observations indicate that WLIM1 colocalizes with the actin cytoskeleton, but not with microtubules, during both interphase and mitosis.

The WLIM1-GFP Network Is Affected by Latrunculin B but Not by Oryzalin

The behavior of the WLIM1-GFP protein was investigated in the presence of latrunculin B (LatB), an inhibitor of actin polymerization that causes the actin network to disassemble (Morton et al., 2000). BY2 cells expressing WLIM1-GFP were treated with 200 nM LatB for 18 h, labeled with rhodamine-phalloidin, and observed by confocal microscopy. As shown in the merged image (Figure 2P), both the actin network and WLIM1-GFP organization were disrupted, and only short fragments of F-actin were still visible (in yellow).

In a control experiment, we also analyzed the effect of oryzalin, a microtubule-depolymerizing drug, on the WLIM1-GFP–decorated network. After 18 h of cell treatment, most of the cells (~85%) exhibited a normal filamentous WLIM1-GFP structure (Figure 2Q) with no significant changes compared with that of untreated cells (Figure 1B). As a proof of oryzalin activity, an increased ratio of cells (13% compared with 5% in nontreated cells) displayed a fluorescence pattern typical of that of the actin cytoskeleton during metaphase (Figure 2R). Strikingly, WLIM1-GFP decorated a structure resembling the two actin bands, called twin peaks, that recently have been shown to form during metaphase in live BY2 cells (Sano et al., 2005). Arrest in metaphase is in line with the well-known effect of oryzalin-induced microtubule depolymerization on the cell cycle (Morejohn et al., 1987). In conclusion, these observations confirm the colabeling of WLIM1-GFP with the actin network, but not with microtubules, and demonstrate that the filamentous network observed for WLIM1-GFP entirely depends on the integrity of the actin cytoskeleton.

Recombinant WLIM1 Interacts Directly with F-Actin in Cosedimentation Assays

The 6xHis-tagged WLIM1 (WLIM1-6His) was expressed in *Escherichia coli* and affinity purified on a nickel-nitrilotriacetic acid agarose (Ni-NTA) matrix. The ability of WLIM1-6His to bind to F-actin was assayed in high-speed (200,000*g*) cosedimentation assays. WLIM1-6His was incubated 1 h with polymerized

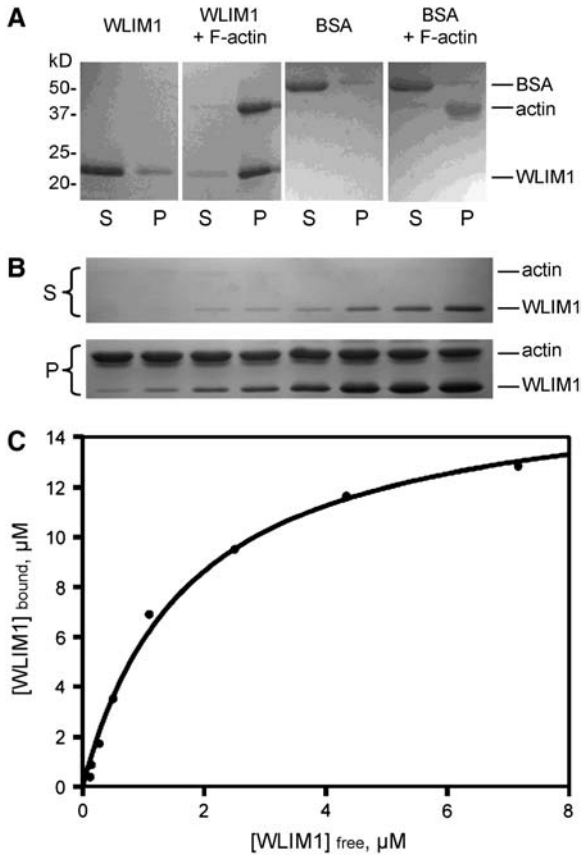

Figure 3. WLIM1 Binds Directly to F-Actin.

(A) High-speed cosedimentation assay. WLIM1 (1 mg mL^{-1}) or control BSA (1 mg mL^{-1}) were incubated with or without F-actin (1 mg mL^{-1}) and centrifuged at 200,000*g* for 45 min. Subsequently, pellets (P) and supernatants (S) were analyzed by SDS-PAGE. WLIM1 bound to F-actin as indicated by its presence in the actin pellet after centrifugation. Control BSA did not cosediment with F-actin.

(B) Increasing concentrations of WLIM1 (0.5 to 20 μM) were cosedimented with 8 μM F-actin and analyzed by SDS-PAGE.

(C) After gel quantification, the concentration of bound WLIM1 was plotted against the concentration of free WLIM1 and fitted with a hyperbolic function. For this representative experiment, the K_d value was 1.49 μM with a stoichiometry at saturation of 1.8 molecules of WLIM1 bound per 1 actin subunit.

F-actin, the mixture was centrifuged, and the resulting pellet and supernatant fractions were analyzed by SDS-PAGE. As shown in Figure 3A, WLIM1-6His was found enriched in the pellet together with F-actin. By contrast, when WLIM1-6His was centrifuged alone, only traces of protein aggregates were detected in the pellet fraction. Finally, control BSA remained in the supernatant in both the absence and presence of F-actin. These data demonstrate that WLIM1 can interact directly with F-actin in vitro.

The affinity of WLIM1 for binding to F-actin was determined by incubating increasing concentrations of WLIM1 with preassembled F-actin. After centrifugation, the amount of WLIM1 in the supernatant and pellet fractions (Figure 3B) was quantified by densitometry. F-actin–bound WLIM1 was plotted against free WLIM1 as exemplified in Figure 3C for a representative experiment. A K_d value of 1.49 μM was obtained by fitting the representative experimental data with a hyperbolic function. At saturation, the stoichiometry of the interaction was 1.8:1 (WLIM1:actin). From three such experiments, a mean dissociation constant ($K_d \pm$ SD) value of 1.27 ± 0.2 μM and a stoichiometry at saturation of 1.9 ± 0.19 mol WLIM1 bound per 1 mol actin were calculated.

In BY2 Cells, the Interaction between GFP-WLIM1 and F-Actin Is Highly Dynamic

The in vivo dynamics of the WLIM1-GFP/actin interaction and the flux of WLIM1-GFP between two distant cytoplasmic regions were assessed in transgenic BY2 cells by fluorescence recovery after photobleaching (FRAP) and fluorescence loss in

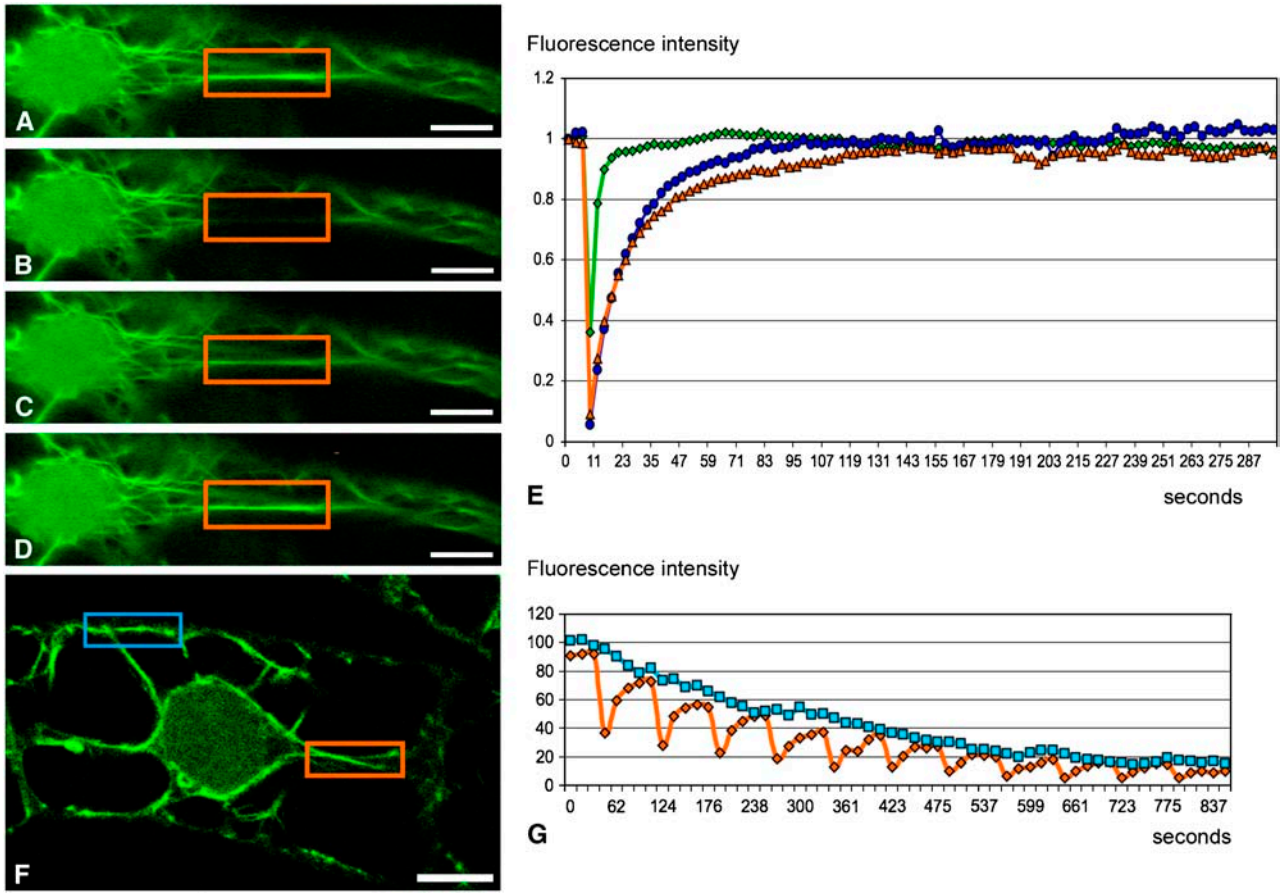

Figure 4. Dynamics of WLIM1-GFP–Actin Interaction.

(A) to **(E)** FRAP experiment.

(A) to **(D)** Fluorescence recovery along bleached WLIM1-GFP filaments. Pictures were recorded before the bleaching **(A)**, immediately after bleaching **(B)**, and 10 **(C)** and 100 **(D)** s after bleaching. The orange rectangle indicates the position of the bleached area.

(E) Quantitative analysis of FRAP in WLIM1-GFP cells (orange curve) in free GFP cells (green curve) and YFP-Talin cells (blue curve). The fluorescence at *t*1/2 was graphically determined: 11 s for LIM and talin and 2.2 s for free GFP.

(F) and **(G)** FLIP experiment.

(F) Prebleached picture indicating the bleached area (orange rectangle) and an unbleached area (blue rectangle) selected to measure fluorescence values in a region distant of the bleached area. Bleach was repeated each five pictures.

(G) Plotted fluorescence intensity in the bleached area (orange curve) and in the distant unbleached area (blue curve). All pictures are single optical 2-μm sections.

Bars = 10 μM.

photobleaching (FLIP), respectively. Figures 4A to 4E show a typical FRAP experiment conducted on a WLIM1-GFP–expressing BY2 cell 24 h after dexamethasone induction. The bleach was applied on a small region of interest (ROI; Figures 4A to 4D, orange rectangle). After photobleaching (Figure 4B), fluorescence recovered within seconds in a pattern resembling the prebleach image, demonstrating that bleaching did not alter actin filament structure (Figures 4C and 4D). The fluorescence level was monitored during 5 min in the ROI, and mean values were plotted (Figure 4E, orange curve). Fluorescence (corrected for bleaching caused by laser scanning during image collection) recovered within 140 s to 100% of the prebleach value. As a comparison, the recovery rates of YFP-mTalin and free GFP were also analyzed and plotted on the same graph (Figure 4E, blue and green curves, respectively). The halftime of recovery ($t1/2$) was very fast for free GFP (i.e., $t1/2 = 2.2 \pm 0.2$ s) and corresponds to the cytoplasmic diffusion of free GFP. By contrast, WLIM1-GFP exhibited a slower but still fast recovery rate of approximately $t1/2 = 11 \pm 3$ s, which was found to be similar to the recovery rate measured for YFP-talin. This value is also consistent with the one previously reported for mTalin in *Arabidopsis thaliana* hypocotyls (Sheahan et al., 2004). FLIP differs from FRAP by the repetitive bleaching of the same region of the specimen. The repetition of the bleaching event progressively depletes the cell of fluorescent molecules that can move into the bleached region, thereby causing a fluorescence loss from unbleached regions. Photobleaching of the ROI (Figure 4F, orange rectangle) was applied until total disappearance of fluorescence in the whole cell. The fluorescence measured in the bleached area (Figure 4F, orange rectangle) and in an unbleached area (Figure 4F, blue rectangle) are plotted in Figure 4G as a function of time. In the bleached area, the fluorescence decreases and recovers at each cycle identically as observed in FRAP experiments. In the unbleached region, the steady loss of fluorescence indicates a continuous exchange of molecules from the two distant regions, and no specific accumulation sites were detected. Together, these data show that rapid exchange of GFP-WLIM1 occurs along actin filaments (FRAP), as expected of side binding proteins existing in equilibrium with nonbound entities, and that nonattached GFP-WLIM1 is rapidly circulated throughout the cytosol (FLIP), as expected for any soluble protein given the high rates of cytoplasmic streaming in plants.

WLIM1 Stabilizes F-Actin in BY2 Cells and in Vitro

The recent data on the vertebrate CRP1 (Tran et al., 2005) and CRP2 (Grubinger and Gimona, 2004) suggest that these proteins may function as stabilizers participating in the regulation of actin cytoskeleton dynamics. This prompted us to test whether WLIM1 could affect the actin cytoskeleton stability following its ectopic expression in tobacco BY2 cells. Kinetics of actin depolymerization induced by LatB (200 nM) in noninduced and dexamethasone-induced WLIM1-GFP–transformed BY2 cells were compared. The actin cytoskeleton was visualized by rhodamine-phalloidin staining before adding LatB and after 10, 40, and 80 min of treatment (Figure 5). As early as 10 min after LatB application, partial depolymerization of the actin cytoskeleton occurred in noninduced cells, while WLIM1-expressing

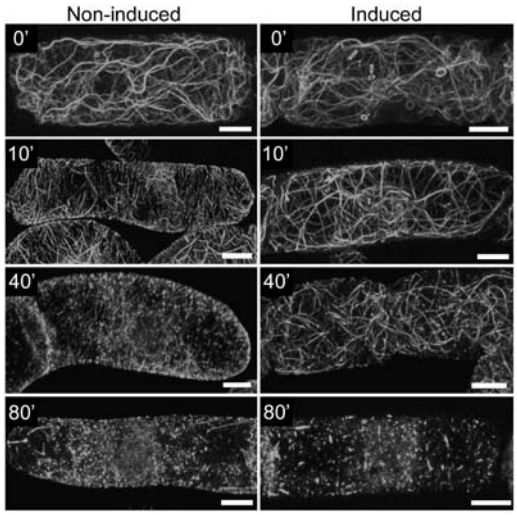

Figure 5. WLIM1 Delays the Effects of LatB in BY2 Cells.

Left column: actin organization in noninduced cells (rhodamine-phalloidin staining) before LatB treatment (0') and after 10 min (10'), 40 min (40'), and 80 min (80'). Right column: actin organization in dexamethasone-induced WLIM1-GFP–transformed cells before LatB treatment (0') and after 10 min (10'), 40 min (40'), and 80 min (80'). Note the presence of filaments 40 min after LatB treatment in WLIM1-expressing cells and their complete disappearance in noninduced cells. Images are projections of x, y, and z optical 0.45-μm sections, respectively. Bars = 10 μm.

cells exhibited an unaffected actin network. After 40 min treatment, 100% of noninduced cells showed a fully depolymerized actin cytoskeleton. By contrast, many intact long actin cables were still present in ~80% of WLIM1-GFP–expressing cells. Finally, after 80 min, nearly all the WLIM1-expressing cells presented a fully disrupted actin cytoskeleton.

The ability of WLIM1 to stabilize actin filaments in an autonomous manner was assessed by in vitro experiments. F-actin was polymerized alone or in the presence of recombinant WLIM1 and subsequently submitted to LatB treatment. Samples were centrifuged at 200,000*g*, and the amount of actin in the resulting supernatants was quantified and expressed as a percentage of total actin (Figures 6A and 6B). As shown in Figure 6B, only 10% of actin was detected in the supernatant of the control sample that has not been treated with LatB. The application of the actin depolymerizing drug resulted in the detection of >45% of actin in the supernatant fraction after 6 h of treatment. By contrast, when actin was polymerized in the presence of WLIM1 prior to the addition of LatB, the proportion of actin in the supernatant decreased proportionally to the WLIM1 concentration, indicating that WLIM1 stabilizes F-actin.

The influence of WLIM1 on the actin filament depolymerization kinetics was also investigated using pyrene-labeled F-actin. After 30 min of polymerization in the absence or in the presence of different amounts of WLIM1, pyrene-labeled F-actin was diluted to a final concentration below the critical concentration of the filament minus end (i.e., 0.4 μM) and the decrease of fluorescence monitored (Figure 7). In the absence of WLIM1, the fluorescence intensity (set at 100% at the beginning of the recording) decreased rapidly, indicating the fast depolymerization

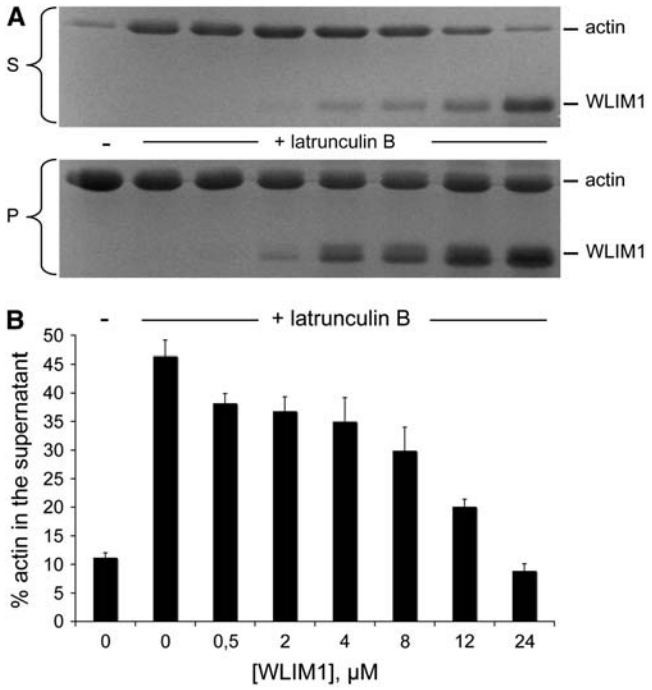

Figure 6. WLIM1 Inhibits the Depolymerization of in Vitro Actin Filaments Induced by LatB.

(A) F-actin (8 μM) was polymerized in absence or presence of different amounts of WLIM1 (0.5 to 24 μM) and subsequently treated with 24 μM LatB. Samples were centrifuged at 200,000*g* for 45 min and the resulting pellets (P) and supernatants (S) analyzed by SDS-PAGE.

(B) The experiments described in **(A)** were repeated three times. The gels were scanned to determine the amount of actin that was present in the supernatant fraction. Data are means ± SD.

of actin filaments. Indeed, after 120 s, the relative fluorescence intensity was 50%. By contrast, when actin filaments were copolymerized with WLIM1, the depolymerization rate was significantly reduced, indicating that WLIM1 stabilizes actin filaments. This stabilization effect was proportional to the amount of WLIM1 and was maximal for a molar ratio of 1:2 (actin:WLIM1).

Overexpression of WLIM1-GFP Modifies the Actin Cytoskeleton Organization in *N. benthamiana* Epidermal Leaf Cells

To investigate whether WLIM1 can modify the actin cytoskeleton organization within a tissue, WLIM1-GFP, and the two actin markers YFP-mTalin (Kost et al., 1998) and the actin binding domain 2 of fimbrin fused to GFP (fABD2-GFP; Sheahan et al., 2004), were used to agroinfiltrate *N. benthamiana* leaves, and the corresponding fluorescent networks were compared. The fluorescent fimbrin and talin-derived actin markers revealed networks similar to those previously described for these fusion proteins in *Arabidopsis* leaf tissues (Sheahan et al., 2004). The fABD2-GFP labeled a dense network of thin and bundled actin filaments in the cortex and in the perinuclear region (Figure 8B). YFP-mTalin displayed broadly similar structures but with small differences. Indeed, a closer analysis revealed that actin filaments were shorter and exhibited an increased branching (Figure 8C). In addition, as expected, YFP-mTalin also accumulated in the nucleus. Consistent with previous observations made in BY2 cells, WLIM1-GFP was found to decorate a cytoskeleton network and to accumulate in the nucleus of leaf epidermal cells (Figure 8A). Importantly, ~100% of the cells that expressed WLIM1-GFP showed a dramatic reduction of the number of actin filaments and bundles and an overall increase of bundle thickness compared with the fABD2-GFP and YFP-mTalin patterns. Although thick actin cables also occasionally formed in the cells that overexpressed fABD2-GFP and YFP-mTalin (data not shown), this was only observed in 20 and 18% of the cells, respectively.

WLIM1 Bundles Actin Filaments

Together, in vivo observations and in vitro results suggest that WLIM1 may function as a bundling protein. To examine further this possibility, low-speed cosedimentation assays were performed. Actin (8 μM) was polymerized alone or in presence of increasing concentrations of WLIM1 (0.25 to 16 μM) and centrifuged for 30 min at 12,500*g*. Samples were analyzed by SDS-PAGE (Figure 9A) and the pelleted actin quantified by densitometric analysis (Figure 9B). In the absence of WLIM1, ~20% of the actin was detected in the pellet. By contrast, in the presence of WLIM1, the amount of actin in the pellet increased proportionally to the WLIM1 concentration, indicating that WLIM1 induces F-actin bundling. A maximum of actin bundling occurred for molar ratios higher than 1:2 (WLIM1:actin). Indeed, for WLIM1 concentrations above 4 μM, ~80% of total actin was detected in the pellet (Figure 9B).

To confirm that WLIM1 induces F-actin bundling, its effects on actin filaments were directly visualized using fluorescence light

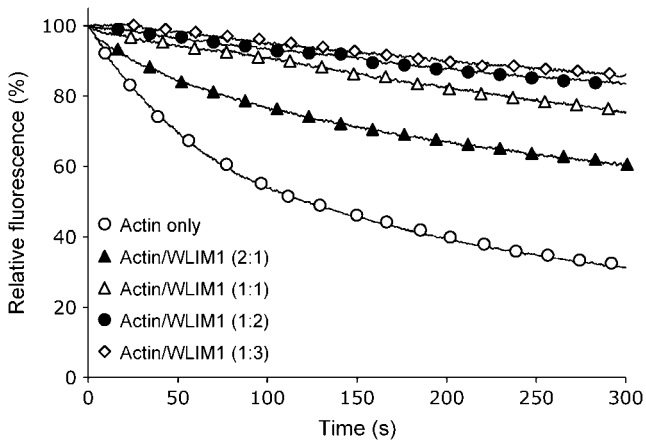

Figure 7. WLIM1 Stabilizes Actin Filaments in Vitro.

A time course of actin filament depolymerization was monitored by pyrene fluorescence. G-actin (4 μM, 25% pyrene labeled) was copolymerized with various concentrations of WLIM1 (2 to 12 μM). Depolymerization was induced by dilution of pyrene-labeled F-actin under the critical concentration of the filament minus end (i.e., 0.4 μM). Fluorescence intensity was set at 100 and recorded over the time. Control was the depolymerization of F-actin in the absence of WLIM1 (open circles).

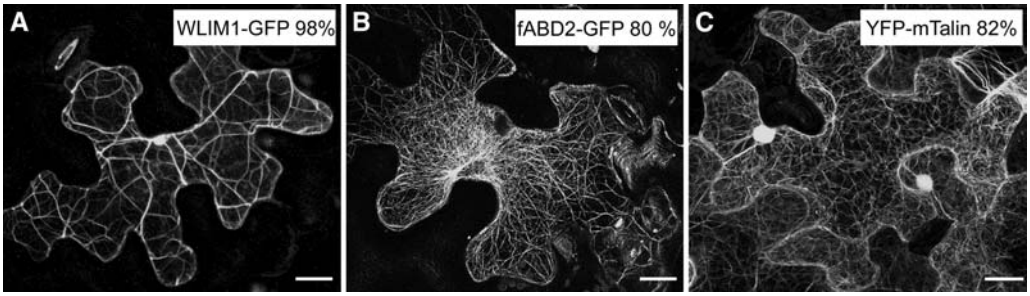

Figure 8. Localization of WLIM1-GFP, Fimbrin ABD2-GFP, and YFP-mTalin in Leaf Epidermal Cells of *N. benthamiana*.

Typical fluorescent patterns observed in the majority of *N. benthamiana* leaf cells (percentage is indicated in the top right corner of pictures) agroinfiltrated with WLIM1-GFP **(A)**, fimbrin ABD2-GFP **(B)**, and YFP-mTalin **(C)**. Notice that, compared with fimbrin ABD2-GFP **(B)** and YFP-mTalin **(C)**, Nt WLIM-GFP **(A)** induces a reduction of the actin filament/bundle number and a thickening of actin bundles/cables. For statistics, ~100 cells from three independent experiments have been scored for each construct. To minimize possible artifacts due to high expression level, observations were made as early as possible after agroinfiltration. Cells that were found to exhibit a higher expression level than the rest of the population and/or to accumulate GFP aggregates (~5% for each construct) were excluded from the scoring. Bars = 10 μm.

microscopy, as shown in Figure 10. In the absence of WLIM1, rhodamine-phalloidin–labeled actin filaments formed a uniform meshwork of fine filaments (Figure 10A). By contrast, when actin was polymerized in the presence of 1 μM WLIM1, higher-order structures were observed (Figures 10B and 10C). Although single actin filaments were still present, most of the actin filaments were recruited into thick and long actin bundles (Figure 10C). Higher magnification allowed recognition of the filaments that formed the bundles (Figure 10D). In the presence of 4 μM or higher concentrations of WLIM1, all actin filaments were incorporated in large aggregated structures, as shown in Figures 10E and 10F. These data demonstrate that WLIM1 displays an autonomous actin bundling activity.

DISCUSSION

The LIM domain defines a tandem zinc-finger structure known to function as a modular protein binding interface. In animals, several LIM proteins, such as the LIM-only and LIM homeodomain proteins, have been found to localize exclusively in the nucleus, where they participate in transcriptional regulation of developmental genes (Jurata et al., 1998; Thaler et al., 2002). Other LIM proteins (e.g., members of the zyxin, EPLIN, enigma, and CRP families) have actin cytoskeleton–associated functions (Louis et al., 1997; Guy et al., 1999; Nix et al., 2001; Maul et al., 2003). In plants, the CRP-related LIM domain–containing proteins (LIMs) form a small multicopy gene family whose biological roles remain unidentified. Based on their expression pattern, plant LIMs can be classified into two subfamilies: the pollen LIMs (PLIMs), which are exclusively and abundantly expressed in pollen grains, and the widely expressed LIMs (WLIMs), which are expressed in all the sporophytic tissues (Eliasson et al., 2000). The high degree of sequence similarity between PLIMs and WLIMs, ranging from 71 to 79% in the case of tobacco, suggests that they represent isoforms. The data presented in this work identify a member of the tobacco CRP-related family, WLIM1, as a new plant F-actin binding protein whose targeting to actin filaments stabilizes the actin cytoskeleton and promotes actin bundle/cable formation.

Confocal analyses showed that WLIM1 accumulates in both the nucleus and the cytoplasm, where it predominantly associates with the actin cytoskeleton. This dual location is in agreement with the one previously reported for the members of the vertebrate CRP family (Arber and Caroni, 1996) and other

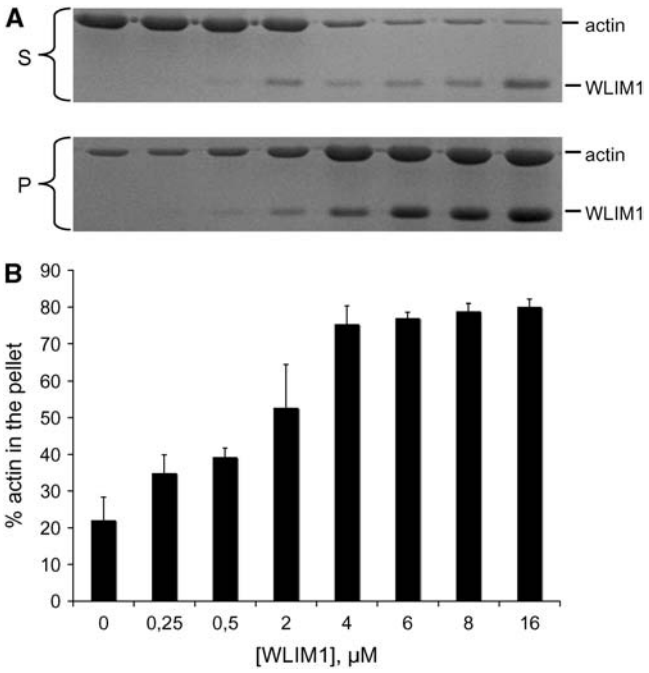

Figure 9. WLIM1 Bundles Actin Filaments in Vitro.

Low-speed cosedimentation assay was used to determine the bundling activity of WLIM1.

(A) Actin at 8 μM alone or in presence of different concentrations of WLIM1 (0.25 to 16 μM) was polymerized and centrifuged at 12,500*g*. The resulting supernatants (S) and pellets (P) were analyzed by SDS-PAGE.

(B) The experiments described in **(A)** were repeated three times. The gels were analyzed to quantify the percentage of actin that sediments in absence or presence of WLIM1. Data are means ± SD.

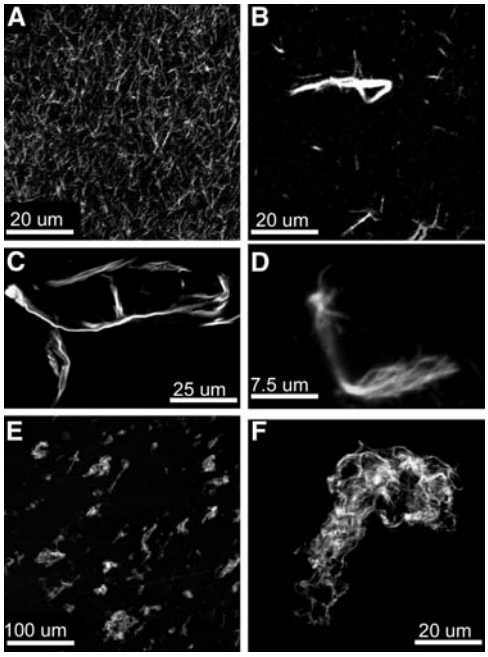

Figure 10. Micrographs of Actin Bundles Polymerized in the Presence of WLIM1.

The effects of WLIM1 on actin filaments were directly visualized by fluorescence light microscopy and rhodamine-phalloidin staining.
(A) Control: actin filaments polymerized in absence of WLIM1.
(B) and **(C)** Bundles of actin filaments formed in presence of 1 μM WLIM1.
(D) High magnification of an actin structure formed in the same conditions as in **(B)** and **(C)**.
(E) and **(F)** Higher-order structures/aggregates formed in presence of 4 μM WLIM1.

CRP-related proteins, such as *Drosophila* Mlp (Stronach et al., 1996) and *Dictyostelium* LimC and D (Khurana et al., 2002). Although CRPs were first believed to interact indirectly with the actin cytoskeleton via intermediary proteins, such as zyxin (Sadler et al., 1992) and α-actinin (Pomiès et al., 1997), recent work has demonstrated that the vertebrate CRP1 (Tran et al., 2005) and CRP2 (Grubinger and Gimona, 2004) are autonomous ABPs. Our in vitro results extend this property to the tobacco WLIM1 protein, suggesting that all CRPs and CRP-related proteins have the ability to associate with F-actin. So far, none of the animal CRPs were reported to interact with microtubules. By contrast, immunolocalization studies of the endogenous WLIM1 protein in sunflower protoplasts have identified this protein in punctuate structures distributed along microtubule bundles (Brière et al., 2003). In light of our observations in live and fixed tobacco cells and tissues, we believe that this does not reflect a real in vivo interaction between the sunflower WLIM1 and microtubules but is rather an artifact resulting from the use of detergents (Nonidet P-40 and Triton) for cell fixation and immunolocalization. As already stated in Results, we observed that Nonidet P-40 and Triton induced a mislocalization of the WLIM1 protein; we did not detect a WLIM1/microtubule association when cells were not treated with a detergent.

The participation of plant LIM proteins in actin-based mechanisms has been indirectly suggested by several observations (Baltz et al., 1999; Mundel et al., 2000). Here, we demonstrate the ability of a plant LIM protein to interact with F-actin in a direct manner and with a high affinity (apparent K_d is 1.27 ± 0.2 μM). As explored by high-speed cosedimentation, we found a stoichiometry at saturation of 1.9 ± 0.19 mol WLIM1 per mol of actin subunit. This result is well supported by the pyrene fluorescence assays that show a maximum of F-actin stabilization for a molecular ratio around 2:1 (WLIM1:actin).

In plant cells, the formation of higher-order actin structures, such as bundles and cables, is crucial to stabilize the organization of transvacuolar strands and maintain the overall cellular architecture (Shimmen et al., 1995). Additionally, these structures represent the tracks for cytoplasmic streaming and organelle and vesicle movements. As mentioned above, a subset of plant LIM proteins, namely the PLIM proteins, which are specifically and highly expressed in germinating pollen grains (Eliasson et al., 2000; Sweetman et al., 2000), may participate in the formation and/or maintaining of long actin cables present in pollen tubes. Consistent with this hypothesis, we observed that ectopic expression of WLIM1 in BY2 cells stabilizes actin filaments/bundles against LatB. In addition, overexpression of WLIM1 in leaf epidermal cells induces both a dramatic decrease of the overall number of actin filaments/bundles and a concomitant thickening of actin bundles. High expression levels of the actin markers fABD2-GFP and YFP-mTalin previously have been reported to induce artificial actin aggregation and/or bundling (Kost et al., 1998; Ketelaar et al., 2004; Sheahan et al., 2004; Voigt et al., 2005; Wilsen et al., 2006). Although a few leaf cells agroinfiltrated with fABD2-GFP or YFP-mTalin exhibited a higher actin bundling level than the rest of the leaf cell population, the effects induced by WLIM1 were much more generalized and pronounced. As stated in Results, ~100% of the cells expressing WLIM1-GFP presented a very high actin bundling level, whereas only 20% of cells expressing fABD2-GFP or YFP-mTalin display a similar phenotype. F-actin stabilization and bundling can be explained by different molecular mechanisms, including the regulation of actin-modulating protein activities. As an example, GFP-mTalin has been shown to affect actin cytoskeleton organization by inhibiting the actin severing activity of ADF (Ketelaar et al., 2004). This prompted us to investigate whether WLIM1 stabilizes and bundles actin filaments directly. In vitro LatB experiments and pyrene fluorescence assays demonstrated that WLIM1 stabilizes F-actin by itself. In addition, low-speed cosedimentation assays and the direct observation of in vitro actin filaments that have been polymerized in the presence of WLIM1 demonstrated that WLIM1 bundles actin filaments in an autonomous manner. So far, only two families of actin bundling proteins have been characterized in plants (i.e., the fimbrins [Kovar et al., 2000] and the villins [Huang et al., 2005]). These data reveal the existence of a third group that includes WLIM1.

The plasticity of the actin cytoskeleton mainly relies on the ability of actin filaments to form, branch, bundle, and disassemble within short timescales in response to many signals. Similarly to GFP-mTalin (Ketelaar et al., 2004), WLIM1 was found both to associate with the actin cytoskeleton in a very dynamic manner and to circulate rapidly throughout the cytoplasm, making it

therefore available where ever and whenever needed for new actin bundle formation.

ABPs either contain two discrete actin binding domains within their sequence (e.g., fimbrin/plastin members; de Arruda et al., 1990) or form multimers that contain a single binding domain per subunit (e.g., α-actinin; Mimura and Asano, 1986). On the one hand, each of the two LIM domains present in plant LIM protein and CRP sequences could display an intrinsic actin binding activity, allowing the monomeric form of plant LIMs and CRPs to bundle actin filaments. On the other hand, animal CRPs and plant LIM proteins may only have a single actin binding site and would require dimer formation to trigger their actin bundling activity. Several LIM proteins, including animal CRPs, have been shown to dimerize through their LIM domains (Feuerstein et al., 1994; Arber and Caroni, 1996). The dimerization of WLIM1 would be in agreement with the observation that, at saturation, 2 mol WLIM1 binds per 1 mol actin subunits; however, this remains to be further demonstrated.

In conclusion, we report here a detailed study of the subcellular localization of a plant LIM protein in living cells. Tobacco WLIM1 is clearly targeted to the actin cytoskeleton but not to microtubules. In vitro results demonstrate that WLIM1 interacts with the filamentous actin in a direct manner and with a high affinity. WLIM1 enhances the stability of the actin cytoskeleton and promotes actin bundling. Together with the recent in vitro data showing that the vertebrate CRP1 protein is able to autonomously bundle actin filaments (Tran et al., 2005), our results indicate that CRPs and the related plant LIMs are a new class of ABPs. Although the exact contribution of plant LIM proteins to the actin cytoskeleton dynamics/remodeling remains to be explored, these data provide strong evidence that plant LIMs are actin cytoskeleton organizers. An open question is the significance of plant LIMs in the nucleus. Several LIM proteins have been shown to shuttle between the cytoplasm and the nucleus and have been suggested to mediate communication between both compartments (see Kadrmas and Beckerle, 2004). Similar functions for plant LIM proteins cannot be excluded. Consistent with a nuclear role for plant LIM proteins, the tobacco protein WLIM1 has been reported to interact with the Pal-box, a *cis*-acting element for several phenylpropanoid synthetic genes (Kawaoka et al., 2000). Finally, the identification of plant LIM protein partners and the analysis of the actin cytoskeleton dynamics and organization in *Arabidopsis* mutants defective in individual or multiple LIMs are currently being conducted in our lab and should provide a better picture of the molecular environment required for LIM protein activity.

METHODS

Generation of Plasmid Constructs Used in This Study

The plasmids used for the transformation of BY2 cells and *Nicotiana benthamiana* plants are derived from an in-house-constructed group of plasmids (pNTL2103 and pNTL3103) produced by assembling the regulatory regions (35S promoter and nos terminator) and the fused coding sequences of GFP, WLIM1, a double HA epitope, and a 6xHis tag, all in a derivative of pBluescript II KS− (Stratagene). These plasmids also contain unique *Xho*I and *Spe*I sites flanking the fused coding sequences, thereby allowing excision of the fragment of interest and its cloning in the *Xho*I-*Spe*I–cleaved pTA7002 plasmid (Aoyama and Chua, 1997). The pNTL2103 and pNTL3103 plasmids differ merely by the nature of the fusion in that the former produces the N-terminal GFP fusion (GFP-WLIM1-2HA-H6) and the latter the C-terminal GFP fusion (WLIM1-GFP-2HA-H6). The YFP-Talin gene construct was supplied by Benedict Kost (University of Heidelberg, Germany). The gene was amplified by PCR and was subcloned in the *Xho*I-*Spe*I sites of the pTA7002 plasmid to give pTA7002-YFP-Talin. The mRFP-WLIM1 construct was obtained by replacing the GFP sequence in the pNTL2103 plasmid by the mRFP gene (Campbell et al., 2002) in the *Nhe*I-*Nco*I sites. Then, the complete coding sequence (mRFP-WLIM1) was subcloned in the *Xho*I-*Spe*I sites of the pTA7002 plasmid to yield the plasmid pTA7002-mRFP-WLIM1. All clones obtained were verified by sequence analysis.

Tobacco BY2 Cell Transformation and Culture

Clonal BY2 tobacco cells (*Nicotiana tabacum* cv BY2; Nagata et al., 1992) transgenic for the pTA7002-GFP-WLIM1, pTA7002-YFP-mTalin, and PTA7002-mRFP-WLIM1 constructs were established by *Agrobacterium tumefaciens*–mediated transformation (Criqui et al., 2000). Expression of GFP-WLIM1 in the transgenic cell lines was induced by the addition of 10 μM dexamethasone to the BY2 culture medium. Selection of cell lines was based on epifluorescence screening of individual transformed calli. Cells were then maintained in liquid BY2 medium under standard conditions. For each experiment, 4 mL of 3-d-old BY2 cells were cultured in a six-well plate and treated as needed.

Agroinfiltration of Leaves

Agrobacterium containing the pTA7002-GFP-WLIM1 or pTA7002-YFP-mTalin or pK7FWG2-fABD2-GFP constructs were grown to saturation in Luria-Bertani medium. Cultures were centrifuged and resuspended in 10 mM $MgCl_2$, 10 mM MES, and 150 μM acetosyringone and kept at room temperature for 2 h. The cultures were then diluted to 1 OD_{600} unit and coinfiltrated into the abaxial side of a young leaf using a 2-mL syringe without the needle. For the inducible constructs,(i.e., pTA7002-GFP-WLIM1 and pTA7002-YFP-mTalin), plants were sprayed 3 d after infiltration with an aqueous solution containing 30 μM dexamethasone and 0.01% Tween 20. Samples were collected as soon as the fluorescence intensity was sufficient to conduct confocal analyses (<10 h after induction). For the pK7FWG2-fABD2-GFP construct, which contains the 35S promoter, observations were also made as soon as the fluorescence intensity was sufficient to conduct confocal analyses (<3 d after infiltration). For each construct, ~100 cells have been observed and scored for the presence of thick actin bundles in three independent experiments.

Staining and Immunolabeling

The actin staining was performed using phalloidin probes as described by Traas et al. (1987). Briefly, 1 volume of a 3-d-old BY2 culture was incubated 15 min in 1 volume of 50 mM PIPES, 50 mM EGTA, 20 mM $MgCl_2$, 5% DMSO, and 0.01% Nonidet P-40, pH 6.9, supplemented with 1 μM rhodamine-phalloidin (Molecular Probes) and DAPI (1 μg/mL) if needed.

For immunolabeling, BY2 cells (24 h after induction) were harvested and allowed to settle onto poly-L-lysine–coated slides, and cells were fixed with 1% glutaraldehyde in culture medium for 15 min at room temperature. The slides were rinsed three times with BY2 medium and treated with cell wall enzymes (0.1% pectolyase and 1% cellulase RS) for 15 min. After washing, slides were incubated overnight in PBS containing freshly prepared 0.1% (w/v) sodium borohydride ($NaBH_4$) to permeabilize the cells and reduce the autofluorescence induced by glutaraldehyde. A blocking step was then performed for 1 h at room temperature in a solution consisting of PBS, 5% BSA, 5% normal goat serum, and 0.1% cold water fish skin gelatin (Aurion). Cells were incubated overnight at 4°C

in a dark, moist chamber in the presence of antitubulin mouse antibodies (Molecular Probes; diluted at 1/300 in PBS and 0.5% BSA), washed four times in PBS, and further incubated in the dark for 4 h at RT with the secondary antibodies (goat anti-mouse IgG1–Alexa 568 nm; diluted 1/300 in PBS and 0.5% BSA; Molecular Probes). Finally, the cells were washed four times with PBS before confocal laser scanning microscopy observation. Control experiments were performed in the absence of primary antibodies to verify the specificity of the labeling.

Drug Treatments

Cytoskeletal inhibitors were added 8 h after induction at the following concentrations: 10 μM oryzalin and 200 nM LatB. Observations were performed 18 h after the addition of the inhibitors. For protection experiments, BY2 cells (24 h after induction) or wild-type cells were harvested and allowed to settle onto poly-L-lysine–coated slides. Fresh medium containing LatB 200 nM was added to the cells that were then incubated for 10, 20, 40, or 80 min. At the end of the incubation time, actin was labeled with rhodamine-phalloidin as described above.

Confocal Laser Scanning Microscopy

Before observation, fixed cells were mounted in a chamber containing PBS and 0.1% Na ascorbate, pH 7.4, to reduce photobleaching. Living cells were allowed to settle onto a poly-L-lysine–coated cover slide before mounting between a cover slip. Pieces of leaves were cut and directly mounted between slides in a water drop. Cells were observed with a Zeiss LSM510 laser scanning confocal microscope using a C-Aprochromat (×63 1.2 numerical aperture water immersion lens) in multitrack mode. Excitation wavelengths and emission filters were 405 nm/band-pass 420 to 480 nm for DAPI, 488 nm/band-pass 505 to 530 nm for GFP or YFP, and 543 nm/long-pass 560 nm for rhodamine, Alexa-Fluor 568, or mRFP. The images are presented as single sections or stacks of neighboring sections as stated in the figure legends. LSM510 three-dimensional reconstruction functions were used to compute projections of serial confocal sections. Image processing was performed using LSM510 version 3.2 (Zeiss) and Photoshop 6.0 (final image assembly; Adobe Systems).

For FRAP experiments, an ×40 oil immersion lens was used, and the confocal pinhole was set to produce optical sections ~2-μm thick. Prebleach and recovery images were acquired at a rate of one image every 3 s. For photobleaching, all argon laser lines (458, 477, 488, and 514 nm) were used simultaneously at 100% transmittance for 40 iterations to bleach an area of ~36 μm^2 always horizontally oriented. Confocal image analysis was performed using the Zeiss LSM software mean ROI function and results tabulated, calculated, and plotted in Microsoft Excel. Loss in fluorescence intensity caused by laser scanning during image collection was corrected and normalized as described by Rabut and Ellenberg (2005). Each graph presented in the figure is an average of 10 experiments. The halftime (*t*1/2) of recovery was determined graphically and corresponds to the time necessary to recover 50% of the fluorescence. For FLIP experiments, bleaching was performed in the same conditions as for FRAP; however, images were acquired at a rate of one image every 13 s to limit the bleaching due to laser exposition. The bleaching was repeated every 75 s.

High- and Low-Speed Cosedimentation Assays

The tobacco WLIM1 coding sequence was subcloned into the pQE-60 plasmid (Qiagen). The 6xHis-tagged WLIM1 was expressed in M15 bacteria and purified using a Ni-NTA resin following procedures described by the manufacturer. The purified protein was concentrated in a centrifugal filter (Amicon) and buffer-exchanged (100 mM NaH_2PO_4 and 10 mM Tris-HCl, pH 7.4) using a 10 K molecular weight cutoff dialysis cassette (Pierce). Rabbit muscle actin (Cytoskeleton) was diluted at 2 mg/mL in A-buffer (5 mM Tris-HCl, pH 8.0, 0.2 mM $CaCl_2$, 0.2 mM Na_2ATP, and 0.5 mM DTT). Polymerization was induced by the addition of actin polymerization inducer (final concentration of 2 mM $MgCl_2$, 1 mM ATP, and 50 mM KCl). Proteins were preclarified at 100,000*g* prior to an experiment. BSA (Sigma-Aldrich) or WLIM1 (1 mg mL^{-1}) were mixed with preassembled F-actin (1 mg mL^{-1}), incubated at 25°C for 1 h, and pelleted at 200,000*g* for 45 min in an Optima TLX ultracentrifuge (Beckman) at 4°C. After the supernatant was removed, protein sample buffer was added to the supernatant and the pellet. Equal amounts of pellet and supernatant samples were analyzed by 12% SDS-PAGE and Coomassie Brillant Blue R (Sigma-Aldrich) staining.

To determine K_d, increasing amounts of WLIM1 (0.5, 1, 2, 4, 8, 12, 16, and 20 μM) were incubated with 8 μM preassembled F-actin for 1 h at 25°C. Samples were analyzed as described above, and the amount of WLIM1 in the pellets or supernatants was quantified using ImageJ v1.37b software (National Institutes of Health). A K_d value and moles of WLIM1 bound per moles of actin subunits at saturation were calculated by fitting the data of bound protein versus free protein to a hyperbolic function with Sigmaplot v10 software (Systat Software).

High-speed cosedimentation assays were also used to determine the effects of LatB on F-actin stabilizing activity of WLIM1. In these experiments, 8 μM actin was polymerized during 1 h at 25°C in the presence of different amounts of WLIM1 (0.5 to 24 μM) before the addition of 24 μM LatB. After 6 h of incubation, samples were centrifuged at 200,000*g* for 45 min and analyzed by SDS-PAGE as previously described. After quantification, results were expressed as percentage of actin in the supernatant as a function of WLIM1 concentration.

In low-speed cosedimentation assays, increasing amounts of WLIM1 (0.25 to 16 μM) were incubated with 8 μM preassembled F-actin for 1 h at 25°C. Samples were centrifuged at 12,500*g* for 30 min in a microcentrifuge at 4°C and analyzed by SDS-PAGE as previously described. After quantification, results were expressed as percentage of actin in the pellet in function of WLIM1 concentration.

F-Actin Depolymerization Assay

Pyrene-labeled F-actin filaments (4 μM, 25% pyrene labeled) were polymerized at room temperature by a 30-min incubation in F-buffer (0.5 mM Tris-HCl, pH 7.5, 0.1 mM $CaCl_2$, 30 mM KCl, 1 mM $MgCl_2$, 2 mM EGTA, 10 mM imidazole, 0.1 mM ATP, and 0.2 mM DTT) in the absence or presence of different amounts of WLIM1 (2 to 12 μM). To induce depolymerization, F-actin was diluted in F-buffer to a final concentration of 0.4 μM. The fluorescence decrease was recorded over the course of 300 s using an F-4500 fluorimeter (Hitachi; excitation at 365 nm and emission at 388 nm).

Fluorescence Microscopy of Actin Filaments

Actin, at 4 μM, alone or in presence of WLIM1, was polymerized in 5 mM Tris-HCl, pH 8.0, 50 mM KCl, 2 mM $MgCl_2$, 0.2 mM $CaCl_2$, 1 mM ATP, and 0.5 mM DTT and labeled with 4 μM of rhodamine-phalloidin (Sigma-Aldrich) during polymerization. Prior to observation, 1 μL of sample was diluted in one drop of cityfluor (Agar Scientific) and applied to a cover slip coated with poly-L-lysine (0.01%). Images were recorded with a Zeiss LSM510 laser scanning confocal microscope using a pinhole set to produce optical sections ~2-μm thick.

Accession Numbers

Sequence data from this article can be found in the GenBank/EMBL data libraries under accession numbers AF184109 (*N. tabacum* WLIM1) and Y11002 (*N. tabacum* WLIM2).

Supplemental Data

The following material is available in the online version of this article.

Supplemental Figure 1. Analysis of WLIM Expression in BY2 Cells.

ACKNOWLEDGMENTS

We thank B. Kost (University of Heidelberg, Germany) for providing the YFP-Talin construct and D. McCurdy (University of Newcastle, Australia) for the GFP-fABD2 construct. This work was supported by the Ministry of Culture, Higher Education, and Research, by the National Research Fund (Luxembourg), and by Grant G.0157.05 of the Fonds voor Wetenschappelijk Onderzoek-Vlaanderen to M.V.T. and C.A.

Received January 13, 2006; revised June 22, 2006; accepted July 13, 2006; published August 11, 2006.

REFERENCES

Aoyama, T., and Chua, N. (1997). A glucocorticoid-mediated transcriptional induction system in transgenic plants. Plant J. **11,** 605–612.

Arber, S., and Caroni, P. (1996). Specificity of single LIM motifs in targeting and LIM/LIM interactions in situ. Genes Dev. **10,** 289–300.

Baltz, R., Evrard, J.L., Domon, C., and Steinmetz, A. (1992). A LIM motif is present in a pollen-specific protein. Plant Cell **4,** 1465–1466.

Baltz, R., Schmit, A.C., Kohnen, M., Hentges, F., and Steinmetz, A. (1999). Differential localization of the LIM domain protein PLIM-1 in microspores and mature pollen grains from sunflower. Sex. Plant Reprod. **12,** 60–65.

Brière, C., Bordel, A.C., Barthou, H., Jauneau, A., Steinmetz, A., Alibert, G., and Petitprez, M. (2003). Is the LIM-domain protein HaWLIM1 associated with cortical microtubules in sunflower protoplasts? Plant Cell Physiol. **44,** 1055–1063.

Campbell, R.E., Tour, O., Palmer, A.E., Steinbach, P.A., Baird, G.S., Zacharias, D.A., and Tsien, R.Y. (2002). A monomeric red fluorescent protein. Proc. Natl. Acad. Sci. USA **99,** 7877–7882.

Chen, C.Y., Wong, E.I., Vidali, L., Estavillo, A., Hepler, P.K., Wu, H.M., and Cheung, A.Y. (2002). The regulation of actin organization by actin-depolymerizing factor in elongating pollen tubes. Plant Cell **14,** 2175–2190.

Criqui, M.C., Parmentier, Y., Derevier, A., Shen, W.H., Dong, A., and Genschik, P. (2000). Cell cycle-dependent proteolysis and ectopic overexpression of cyclin B1 in tobacco BY2 cells. Plant J. **24,** 763–773.

de Arruda, M.V., Watson, S., Lin, C.S., Leavitt, J., and Matsudaira, P. (1990). Fimbrin is a homologue of the cytoplasmic phosphoprotein plastin and has domains homologous with calmodulin and actin gelation proteins. J. Cell Biol. **111,** 1069–1079.

Dong, C.H., Xia, G.X., Hong, Y., Ramachandran, S., Kost, B., and Chua, N.H. (2001). ADF proteins are involved in the control of flowering and regulate F-actin organization, cell expansion, and organ growth in *Arabidopsis.* Plant Cell **13,** 1333–1346.

Eliasson, A., Gass, N., Mundel, C., Baltz, R., Kräuter, R., Evrard, J.L., and Steinmetz, A. (2000). Molecular and expression analysis of a LIM protein gene family from flowering plants. Mol. Gen. Genet. **264,** 257–267.

Feuerstein, R., Wang, X., Song, D., Cooke, N.E., and Liebhaber, S.A. (1994). The LIM/double zinc-finger motif functions as a protein dimerization domain. Proc. Natl. Acad. Sci. USA **91,** 10655–10659.

Grubinger, M., and Gimona, M. (2004). CRP2 is an autonomous actin-binding protein. FEBS Lett. **557,** 88–92.

Guy, P.M., Kenny, D.A., and Gill, G.N. (1999). The PDZ domain of the LIM protein enigma binds to beta-tropomyosin. Mol. Biol. Cell **10,** 1973–1984.

Huang, S., Robinson, R.C., Gao, L.Y., Matsumoto, T., Brunet, A., Blanchoin, L., and Staiger, C.J. (2005). Arabidopsis VILLIN1 generates actin filament cables that are resistant to depolymerization. Plant Cell **17,** 486–501.

Jurata, L.W., Pfaff, S.L., and Gill, G.N. (1998). The nuclear LIM domain interactor NLI mediates homo- and heterodimerization of LIM domain transcription factors. J. Biol. Chem. **273,** 3152–3157.

Kadrmas, J.L., and Beckerle, M.C. (2004). The LIM domain: From the cytoskeleton to the nucleus. Nat. Rev. Mol. Cell Biol. **5,** 920–931.

Kawaoka, A., Kaothien, P., Yoshida, K., Endo, S., Yamada, K., and Ebinuma, H. (2000). Functional analysis of tobacco LIM protein Ntlim1 involved in lignin biosynthesis. Plant J. **22,** 289–301.

Ketelaar, T., Anthony, R.G., and Hussey, P.J. (2004). Green fluorescent protein-mTalin causes defects in actin organization and cell expansion in *Arabidopsis* and inhibits actin depolymerizing factor's actin depolymerizing activity *in vitro.* Plant Physiol. **136,** 3990–3998.

Khurana, B., Khurana, T., Khaire, N., and Noegel, A.A. (2002). Functions of LIM proteins in cell polarity and chemotactic motility. EMBO J. **21,** 5331–5342.

Kost, B., Spielhofer, P., and Chua, N.H. (1998). A GFP-mouse talin fusion protein labels plant actin filaments *in vivo* and visualizes the actin cytoskeleton in growing pollen tubes. Plant J. **16,** 393–401.

Kovar, D.R., Staiger, C.J., Weaver, E.A., and McCurdy, D.W. (2000). AtFim1 is an actin filament crosslinking protein from *Arabidopsis thaliana.* Plant J. **24,** 625–636.

Louis, H.A., Pino, J.D., Schmeichel, K.L., Pomies, P., and Beckerle, M.C. (1997). Comparison of three members of the cysteine-rich protein family reveals functional conservation and divergent patterns of gene expression. J. Biol. Chem. **272,** 27484–27491.

Maul, R.S., Song, Y., Amann, K.J., Gerbin, S.C., Pollard, T.D., and Chang, D.D. (2003). EPLIN regulates actin dynamics by cross-linking and stabilizing filaments. J. Cell Biol. **160,** 399–407.

McCurdy, D.W., Kovar, D.R., and Staiger, C.J. (2001). Actin and actin-binding proteins in higher plants. Protoplasma **215,** 89–104.

Mimura, N., and Asano, A. (1986). Isolation and characterization of a conserved actin-binding domain from rat hepatic actinogelin, rat skeletal muscle, and chicken gizzard alpha-actinins. J. Biol. Chem. **261,** 10680–10687.

Morejohn, L., Bureau, T., Molé-Bajer, J., Bajer, A., and Fosket, D. (1987). Oryzalin, a dinitroaniline herbicide, binds to plant tubulin and inhibits microtubule polymerization *in vitro.* Planta **172,** 252–264.

Morton, W.M., Ayscough, K.R., and McLaughlin, P.J. (2000). Latrunculin alters the actin-monomer subunit interface to prevent polymerization. Nat. Cell Biol. **2,** 376–378.

Mundel, C., Baltz, R., Eliasson, A., Bronner, R., Gass, N., Kräuter, R., Evrard, J.L., and Steinmetz, A. (2000). A LIM-domain protein from sunflower is localized to the cytoplasm and/or nucleus in a wide variety of tissues and is associated with the phragmoplast in dividing cells. Plant Mol. Biol. **42,** 291–302.

Nagata, T., Nemoto, Y., and Hasezawa, S. (1992). Tobacco BY-2 cell line as the ''HeLa'' cell in the cell biology of higher plants. Int. Rev. Cytol. **132,** 1–30.

Nix, D.A., Fradelizi, J., Bockholt, S., Menichi, B., Louvard, D., Friederich, E., and Beckerle, M.C. (2001). Targeting of zyxin to sites of actin membrane interaction and to the nucleus. J. Biol. Chem. **276,** 34759–34767.

Pomiès, P., Louis, H.A., and Beckerle, M.C. (1997). CRP1, a LIM domain protein implicated in muscle differentiation, interacts with alpha-actinin. J. Cell Biol. **139,** 157–168.

Rabut, G., and Ellenberg, J. (2005). Photobleaching techniques to study mobility and molecular dynamics of proteins in live cells: FRAP, iFRAP, and FLIP. In Live Cell Imaging: A Laboratory Manual, R.D. Goldman and D.L. Spector, eds (Cold Spring Harbor, NY: Cold Spring Harbor Laboratory Press), pp. 101–126.

Sadler, I., Crawford, A.W., Michelsen, J.W., and Beckerle, M.C. (1992). Zyxin and cCRP: Two interactive LIM domain proteins associated with the cytoskeleton. J. Cell Biol. **119,** 1573–1587.

Sano, T., Higaki, T., Oda, Y., Hayashi, T., and Hasezawa, S. (2005). Appearance of actin microfilament 'twin peaks' in mitosis and their function in cell plate formation, as visualized in tobacco BY-2 cells expressing GFP-fimbrin. Plant J. **44,** 595–605.

Schmeichel, K.L., and Beckerle, M.C. (1997). Molecular dissection of a LIM domain. Mol. Biol. Cell **8,** 219–230.

Sheahan, M.B., Staiger, C.J., Rose, R.J., and McCurdy, D.W. (2004). A green fluorescent protein fusion to actin-binding domain 2 of *Arabidopsis* fimbrin highlights new features of a dynamic actin cytoskeleton in live plant cells. Plant Physiol. **136,** 3968–3978.

Shimmen, T., Hamatani, M., Saito, S., Yokota, E., Mimura, T., Fusetani, N., and Karaki, H. (1995). Roles of actin filaments in cytoplasmic streaming and organization of transvacuolar strands in root hair cells of *Hydrocharis.* Protoplasma **185,** 188–193.

Staiger, C.J., Goodbody, K.C., Hussey, P.J., Valenta, R., Drobak, B.K., and Lloyd, C.W. (1993). The profilin multigene family of maize: Differential expression of three isoforms. Plant J. **4,** 631–641.

Stronach, B.E., Siegrist, S.E., and Beckerle, M.C. (1996). Two muscle-specific LIM proteins in Drosophila. J. Cell Biol. **134,** 1179–1195.

Sweetman, J., Spurr, C., Eliasson, A., Gass, N., Steinmetz, A., and Twell, D. (2000). Isolation and characterisation of two pollen-specific LIM domain protein cDNAs from *Nicotiana tabacum.* Sex. Plant Reprod. **12,** 339–345.

Thaler, J.P., Lee, S.K., Jurata, L.W., Gill, G.N., and Pfaff, S.L. (2002). LIM factor Lhx3 contributes to the specification of motor neuron and interneuron identity through cell-type-specific protein-protein interactions. Cell **110,** 237–249.

Traas, J.A., Doonan, J.H., Rawlins, D.J., Shaw, P.J., Watts, J., and Lloyd, C.W. (1987). An actin network is present in the cytoplasm throughout the cell cycle of carrot cells and associates with the dividing nucleus. J. Cell Biol. **105,** 387–395.

Tran, T.C., Singleton, C., Fraley, T.S., and Greenwood, J.A. (2005). Cysteine-rich protein 1 (CRP1) regulates actin filament bundling. BMC Cell Biol. **6,** 45.

Vidali, L., McKenna, S.T., and Hepler, P.K. (2001). Actin polymerization is essential for pollen tube growth. Mol. Biol. Cell **12,** 2534–2545.

Vidali, L., Yokota, E., Cheung, A.Y., Shimmen, T., and Hepler, P.K. (1999). The 135kDa actin-bundling protein from *Lilium longiflorum* pollen is the plant homologue of villin. Protoplasma **209,** 283–291.

Voigt, B., et al. (2005). Actin-based motility of endosomes is linked to the polar tip growth of root hairs. Eur. J. Cell Biol. **84,** 609–621.

Wilsen, K.L., Lovy-Wheeler, A., Voigt, B., Menzel, D., Kunkel, J.G., and Hepler, P.K. (2006). Imaging the actin cytoskeleton in growing pollen tubes. Sex. Plant Reprod. **19,** 51–62.

Yokota, E., Vidali, L., Tominaga, M., Tahara, H., Orii, H., Morizane, Y., Hepler, P.K., and Shimmen, T. (2003). Plant 115-kDa actin-filament bundling protein, P-115-ABP, is a homologue of plant villin and is widely distributed in cells. Plant Cell Physiol. **44,** 1088–1099.